2009 American Control Conference
Hyatt Regency Riverfront, St. Louis, MO, USA
June 10-12, 2009



# Classification of Dynamic Atomic Force Microscopy Control Modes Based on Asymptotic Nonlinear Mechanics

Sergey Belikov and Sergei Magonov

***Abstract*—Control design and improvement of dynamic atomic force microscopy (AFM) modes and development of new dynamic modes are among the central problems of AFM theory and practice. Proper design can speed up the scan, improve quality, and suggest new useful image channels and algorithms for quantitative measurements at the nanometer scale. This paper provides a rigorous modeling based on first principles and mechanical setting of the AFM. A relationship between the empirical "effective" parameters of mass-spring models and the properties of cantilever and mechanical characteristics of the AFM was formulated. KBM averaging method was used to derive asymptotic dynamics with amplitude and phase as the state variables. Two equations for steady state of this asymptotic dynamics have four unknowns – amplitude, phase, height, and frequency shift. Keeping two of four unknown variables constant (and re-solving other two by the equations for steady state) determines six dynamic AFM modes, of which four are widely used. They are amplitude modulation (AM) and frequency modulation (FM) with force spectroscopy and imaging operations. The good match between the simulated and experimental results for AM is found.**

## I. INTRODUCTION

Atomic force microscopy (AFM) [1], which has been introduced as an accessory to scanning tunneling microscopy (STM), has been developed into the leading scanning probe technique. Nowadays, AFM is broadly applied for exploring various materials and phenomena at the nanoscale. In its basic function AFM is used for high-resolution profiling of surfaces and it can be also applied for examination of local mechanical and electromagnetic properties. The core of this method is the force interactions between a minute tip attached to a cantilever and a sample surface. The cantilever response to the tip-sample forces is employed for surface profiling while the probe is pivoted over the surface. Initially, a quasistatic deflection of the cantilever, which is proportional to the force, was used for the force measurement and control when the scanning tip stays in a permanent contact with the sample. Such contact mode has definite limitations in studies of soft materials. Dynamic techniques, in which an oscillating probe comes only into an intermittent contact with a sample, were introduced to overcome this hurdle. Oscillatory AFM is implemented in the amplitude modulation (AM) [2] or frequency modulation (FM) [3] modes, which complement each other in studies of samples in various environments. The AM mode is most applicable for ambient-condition studies and its wide applications to polymers and biological objects made AFM a routine characterization method. Despite the broad acceptance of the AM mode the use of oscillating probe has a serious drawback due to a complicated relationship between the parameters of probe dynamics (amplitude, phase, frequency) and the tip-sample force. For a while a poor knowledge about the tip-sample force interactions in oscillatory modes was compromised by empirical observations and simplified theoretical considerations [4-6]. Recently the use of specialized probes was suggested for either reconstruction of the tip-sample force from harmonics analysis [7-8], or for direct measurements of the tip-sample force during a single oscillation [9]. Although all these efforts are very useful and informative, a rigorous approach towards dynamics of AFM modes is still in demand and this need will be growing further with the development of multifrequency AFM measurements [10]. The multifrequency detection of the probe response is invaluable for studies in complex but frequently occurring practical situations when the forces of different origin (mechanical, electrostatic, magnetic, etc) cause displacements of the same microfabricated probe. A deconvolution of different force contributions can be achieved in the multifrequency approach. For example, surface topography and surface potential can be simultaneously and independently determined with similar and high resolution when a conducting probe operates in the intermittent contact regime [11-12]. This complexity demands the detailed and rigorous consideration of the AFM oscillatory modes, and the treatment of the problem in terms of asymptotic nonlinear mechanics is suggested below. Classification of the oscillatory modes based on this theory provides a background for better understanding of AFM functionality, realistic simulators, improved control design, and quantitative measurements of local properties (mechanical, electrostatic, magnetic, etc.).

## II. MODEL OF AFM CANTILEVER DYNAMICS

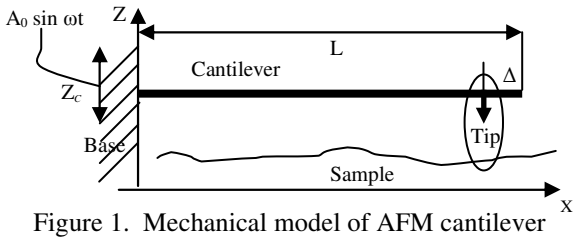


Figure 1. Mechanical model of AFM cantilever with vibrating base

A mechanical model of a controllably oscillated AFM probe that will be considered in the dynamic analysis is

Manuscript received September 15, 2008.
S. Belikov is with Marena Systems Corporation, Hayward, CA 94545
S. Magonov is with Agilent Technologies, Inc., Chandler, AZ 85226

presented in Figure 1. A thin cantilever of length $L$ and cross-section $S = b \times h$ is attached to the base at point $(x = 0, Z = Z_c)$. The base is oscillating as $Z(0,t) = Z_c + A_0 \sin \omega t$. Concentrated forces may be applied to the tip due to tip-sample interaction at the distance $\Delta$ from the edge, i.e. at $x = L - \Delta$; weight of the tip is applied at the same point.

Mathematically this problem can be described by Euler-Bernoulli's type of equation (excellent treatment can be found in [13])

$$\frac{\partial^2 Z(x,t)}{\partial t^2} + 2\beta \frac{\partial Z(x,t)}{\partial t} + a^2 \frac{\partial^4 Z(x,t)}{\partial x^4} = [H(Z(x,t)) - p]\delta(x - (L - \Delta)) \quad \textbf{(1)}$$

with the following boundary conditions.

Base motion:

$$Z(0,t) = Z_c + A_0 \sin \omega t \quad \textbf{(2)}$$

Cantilever is attached to the base:

$$\frac{\partial Z}{\partial x}(0,t) = 0 \quad \textbf{(3)}$$

Free end (no moment):

$$\frac{\partial^2 Z}{\partial x^2}(L,t) = 0 \quad \textbf{(4)}$$

Free end (no force):

$$\frac{\partial^3 Z}{\partial x^3}(L,t) = 0 \quad \textbf{(5)}$$

The following notations (SI units are shown in brackets) are used in (1)-(5):

$L$, $b$, and $h$ [m]-length, width and height of the cantilever;

$\Delta$ [m] –position of the tip from the end of the cantilever;

$x$ [m]-horizontal coordinate;

$Z$ [m]-vertical coordinate;

$Z_c$ [m]-the position where cantilever is attached to the base;

$t$ [sec]-time;

$A_0$[m]-amplitude of base (piezo drive) vibration;

$\omega$ [rad/sec]-frequency of base (piezo drive) vibration;

$Z(x,t)$ [m]-vertical position of the cantilever at point $x$ and time $t$;

$\beta[\sec^{-1}]$- damping coefficient (may depend on $\omega$);

$a^2 = \frac{EI}{\rho S}\left[\frac{\mathrm{m}^4}{\sec^2}\right]$, where

$E\left[\frac{N}{m^2}\right]$-Young's modulus of the cantilever;

$I = \frac{bh^3}{12}[\mathrm{m}^4]$-moment of inertia of the cross-section with respect to horizontal axis;

$\rho\left[\frac{\mathrm{kg}}{\mathrm{m}^3}\right]$-density of the cantilever;

$S = bh[\mathrm{m}^2]$-area of the cross-section of the cantilever;

$H(Z) \times \rho \times 1\mathrm{m} \times S[N]$-concentrated force applied to the tip due to tip-sample interaction;

$p \times \rho \times 1\mathrm{m} \times S\,[N]$ -weight of the tip

$\delta(x)\left[\frac{1}{\mathrm{m}}\right]$-Dirack's delta function.

Ignoring the weight of the tip (which adds only an insignificant technical complication), the motion of the tip located at the position $l = L - \Delta$ near the first resonance is

$$Z(l,t) = Z_c + \eta_1 + \xi_1$$

where $\xi_1$ and $\eta_1$ satisfy the following equations

$$\ddot{\xi}_1 + 2\beta_1 \dot{\xi}_1 + \omega_1^2 \xi_1 = \frac{F\left(Z_c + \eta_1 + \xi_1; \operatorname{sgn}\left(\dot{\eta}_1 + \dot{\xi}_1\right)\right)}{\rho S \left\|Z_1^l\right\|^2} \quad \textbf{(6)}$$

$$\eta_1 = d\cos\left(\omega t + \varphi_d\right) \quad \textbf{(7)}$$

$\omega_1$ is the 1st eigen-frequency of the cantilever [13];

$\beta_1$, calculated by the formula

$$\beta_1 = \frac{\omega_1}{\sqrt{4Q_1^2 - 1}} \approx \frac{\omega_1}{2Q_1} \quad \textbf{(8)}$$

is the damping factor of the cantilever's 1st mode and

$Q_1$ is the quality factor of the 1st mode;

$\|Z_1^l\|$ is a norm of special basis function of the first mode such that $Z_1^l(l) = 1$; the norm has SI unit $[\sqrt{m}]$;

$d$ and $\varphi_d$ are (calculated using Euler-Bernoulli based math) amplitude and phase of the tip's oscillation caused by base oscillation only (usually called "free" oscillation by AFM practitioners), but not by tip-sample interaction; $d$ and $\varphi_d$ depend on $A_0$, $\omega$, $\omega_1$, $\beta_1$, and $\Delta$;

and $F(z;\operatorname{sgn}\dot{z})$ is the tip-sample interaction function at the cantilever position $z$ at the location of the tip; this function defines behavior of the mode; we assume that it depends on direction of the motion $\operatorname{sgn}\dot{z}$; tip-sample interactions will be discussed below in Section IV.

## III. Krylov-Bogoliubov-Mitropolsky (KBM) Averaging for Modeling Oscillating AFM Modes

We assume that

$$\varepsilon = Q_1^{-1} << 1 \quad \textbf{(9)}$$

is small and it is admissible to neglect the values of order of $\varepsilon^2$. We also assume that the difference between driving frequency $\omega$ and the eigen-frequency $\omega_1$ is of the order $\varepsilon$ and define the related parameter of order 1.

$$g = \frac{\omega - \omega_1}{\varepsilon} = Q_1(\omega - \omega_1) \quad \textbf{(10)}$$

These are the natural assumptions for most of practical cases.

We also consider small piezo drive amplitudes, i.e. $A_0 \sim \varepsilon$, then we can show that in (6), (7) $d \sim 1$; and

$$\frac{F(z;\operatorname{sgn}\dot{z})}{\rho S \left\|Z_1^l\right\|^2} \sim \varepsilon$$

The following equation is a direct consequence of (10):

$$\omega^2 - \omega_1^2 = 2\varepsilon g \omega_1 + O(\varepsilon^2) \quad \textbf{(11)}$$

Let us define the function $H$ of the order of 1 as the following

$$H(z;\operatorname{sgn}\dot{z}) = \frac{Q_1}{\rho S \left\|Z_1^l\right\|^2} F(z;\operatorname{sgn}\dot{z}) \quad \textbf{(12)}$$

This function has unit of acceleration, and $H(z;\operatorname{sgn}\dot{z}) \sim 1$. We use the following notations

$$H_a(z)=H(z,-1);\quad F_a(z)=F(z,-1)-\text{approach force;}$$
$$H_r(z)=H(z,+1);\quad F_r(z)=F(z,+1)-\text{reproach force;} \qquad (13)$$

Defining the effective mass by

$$m=\rho S\left\|Z_1^l\right\|^2 \qquad (14)$$

equations (12), (13) become

$$H(z;\operatorname{sgn}\dot z)=\frac{Q_1F(z;\operatorname{sgn}\dot z)}{m},$$
$$H_a(z)=\frac{Q_1F_a(z)}{m},\quad H_r(z)=\frac{Q_1F_r(z)}{m} \qquad (15)$$

Let

$$\xi=\eta_1+\xi_1$$

It is a combined tip's deflection due to the base vibration and the tip-sample interaction. Then equation (6) is equivalent to

$$\ddot\xi+\omega_1^2\xi=\varepsilon\Phi\left(\xi,\dot\xi\right)+\varepsilon f\left(t\right) \qquad (16)$$

with (using (14)-(15))

$$\Phi\left(\xi,\dot\xi\right)=H\left(Z_0+\xi;\operatorname{sgn}\dot\xi\right)-\omega_1\dot\xi \qquad (17)$$

and

$$\varepsilon f(t)=-d\left[\left(\omega^2-\omega_1^2\right)\cos(\omega t+\varphi_d)+2\beta_1\omega\sin(\omega t+\varphi_d)\right]$$

Using (8)-(11), this formula with accuracy of the order $\varepsilon^2$ is equivalent to

$$\varepsilon f(t)=-\varepsilon d\omega_1\left[\omega_1\sin(\omega t+\varphi_d)+2g\cos(\omega t+\varphi_d)\right] \text{ or}$$

$$f(t)=d\omega_1\sqrt{\omega_1^2+4g^2}\cos\zeta \qquad (18)$$

where

$$\zeta=\omega t+\varphi_d+\arccos\frac{\omega_1}{\sqrt{\omega_1^2+4g^2}}+\frac{\pi}{2} \qquad (19)$$

Asymptotic as $\varepsilon\to0$ solution of equation (17) is harmonic with slowly varying amplitude $x$, phase $y$ and large frequency $\omega_1$

Figure 2. Plot of the solution of equation (16) looks like black box for observable time; it has no information besides amplitude and phase of the rapid oscillation

Solution of equation (16), as shown in Figure 2, is close to the rapidly oscillating harmonic function with slowly varying amplitude and phase. The amplitude and phase are the parameters measured by AFM and it is desirable to model AFM dynamics with these state variables. Using van der Pole (amplitude-phase) variables $(x,y)$, defined by [14]

$$\xi=x\cos\ y\qquad \dot\xi=-\omega_1 x\sin\ y \qquad (20)$$

equation (16) can be written in the equivalent form

$$\begin{cases}\dot x=-\dfrac{\varepsilon}{\omega_1}\left[\Phi\left(x\cos y,-\omega_1 x\sin y\right)+f(t)\right]\sin y\\ \dot y=\omega_1-\dfrac{\varepsilon}{\omega_1 x}\left[\Phi\left(x\cos y,-\omega_1 x\sin y\right)+f(t)\right]\cos y\end{cases} \qquad (21)$$

or, substituting $f$ from (18)-(19),

$$\begin{cases}\dot x=-\varepsilon\left[\dfrac{1}{\omega_1}\Phi\left(x\cos y,-\omega_1 x\sin y\right)+d\sqrt{\omega_1^2+4g^2}\cos\zeta\right]\sin y\\ \dot y=\omega_1-\varepsilon\left[\dfrac{1}{\omega_1 x}\Phi\left(x\cos y,-\omega_1 x\sin y\right)\cos y+\dfrac{d\sqrt{\omega_1^2+4g^2}}{x}\cos\zeta\right]\cos y\\ \dot\zeta=\omega\end{cases} \qquad (22)$$

System of differential equations (22) has a slow variable $x$ and two fast variables $y$ and $\zeta$. Introducing a new slow variable (phase difference) as difference between two fast ones,

$$\theta=\zeta-y \qquad (23)$$

equation (22) is equivalent to

$$\begin{cases}\dot x=-\varepsilon\left[\dfrac{1}{\omega_1}\Phi(x\cos(\zeta-\theta),-\omega_1 x\sin(\zeta-\theta))+d\sqrt{\omega_1^2+4g^2}\cos\zeta\right]\sin(\zeta-\theta)\\ \dot\theta=\varepsilon\left\{\left[\dfrac{1}{\omega_1 x}\Phi(x\cos(\zeta-\theta),-\omega_1 x\sin(\zeta-\theta))\cos(\zeta-\theta)+\dfrac{d\sqrt{\omega_1^2+4g^2}}{x}\cos\zeta\right]\cos(\zeta-\theta)+g\right\}\\ \dot\zeta=\omega\end{cases}$$

Applying KBM averaging (over the remaining fast variable $\zeta$) method [14], we obtain asymptotic equation

$$\begin{cases}\dot x=-\dfrac{\varepsilon}{2\pi\omega_1}\left\{\displaystyle\int_0^{2\pi}\Phi(x\cos(\zeta-\theta),-x\omega_1\sin(\zeta-\theta))\sin(\zeta-\theta)d\zeta+d\omega_1\sqrt{\omega_1^2+4g^2}\int_0^{2\pi}\cos\zeta\sin(\zeta-\theta)d\zeta\right\}\\ \dot\theta=\dfrac{\varepsilon}{2\pi\omega_1 x}\left\{\displaystyle\int_0^{2\pi}\Phi(x\cos(\zeta-\theta),-x\omega_1\sin(\zeta-\theta))\cos(\zeta-\theta)d\zeta+d\omega_1\sqrt{\omega_1^2+4g^2}\int_0^{2\pi}\cos\zeta\cos(\zeta-\theta)d\zeta\right\}+\varepsilon g\end{cases}$$

and, after calculating the second integrals, the following equations:

$$\begin{cases}\dot x=-\dfrac{\varepsilon}{2\pi\omega_1}\left\{\displaystyle\int_0^{2\pi}\Phi\left(x\cos y,-x\omega_1\sin y\right)\sin y dy-\pi d\omega_1\sqrt{\omega_1^2+4g^2}\sin\theta\right\}\\ \dot\theta=\dfrac{\varepsilon}{2\pi\omega_1 x}\left\{\displaystyle\int_0^{2\pi}\Phi\left(x\cos y,-x\omega_1\sin y\right)\cos y dy+\pi d\omega_1\sqrt{\omega_1^2+4g^2}\cos\theta\right\}+\varepsilon g\end{cases}$$

To further simplify, we write according to (17) and (20),

$$\Phi\left(x\cos y,-x\omega_1\sin y\right)=H\left(Z_c+x\cos y;-\operatorname{sgn}\sin y\right)+\omega_1^2 x\sin y$$

and, using (13),(14),(15),

$$\begin{cases}\dot x=-\dfrac{\varepsilon}{2\pi\omega_1}\left\{\dfrac{Q_1}{m}\displaystyle\int_0^{\pi}\left[F_a-F_r\right]\left(Z_c+x\cos y\right)\sin y dy+\pi\omega_1^2 x-\pi d\omega_1\sqrt{\omega_1^2+4g^2}\sin\theta\right\}\\ \dot\theta=\dfrac{\varepsilon}{2\pi\omega_1 x}\left\{\dfrac{Q_1}{m}\displaystyle\int_0^{\pi}\left[F_a+F_r\right]\left(Z_c+x\cos y\right)\cos y dy+\pi d\omega_1\sqrt{\omega_1^2+4g^2}\cos\theta\right\}+\varepsilon g\end{cases} \qquad (24)$$

This is the main equation of oscillatory AFM dynamics and can be used for an efficient simulation, as a plant for control systems design, and many other applications. In this paper it is used for the definition and classification of oscillatory AFM modes and for interplay between theory and experiment.

Steady-state solutions of (24) for amplitude and phase $(x,\theta)$ satisfy the following system of equations

$$\begin{cases} \sin\theta = \dfrac{1}{\sqrt{1+\left(\dfrac{2g}{\omega_1}\right)^2}}\left\{\dfrac{1}{N}\int_0^{\pi}[F_a - F_r](Z_0 + x\cos y)\sin y dy + \dfrac{x}{d}\right\} \\ \cos\theta = -\dfrac{1}{\sqrt{1+\left(\dfrac{2g}{\omega_1}\right)^2}}\left\{\dfrac{1}{N}\int_0^{\pi}[F_a + F_r](Z_0 + x\cos y)\cos y dy + \dfrac{2g}{\omega_1}\dfrac{x}{d}\right\} \end{cases} \quad (25)$$

where

$$N = \pi d\omega_1^2 Q_1^{-1} m \quad (26)$$

can be called normalizing force. Using the notation

$$\begin{cases} \mathrm{Si}_0^{[F_a-F_r]}(Z_c,x) = \dfrac{1}{N}\int_0^{\pi}[F_a - F_r](Z_c + x\cos y)\sin y dy + \dfrac{x}{d} \\ \mathrm{Co}_0^{[F_a+F_r]}(Z_c,x) = -\dfrac{1}{N}\int_0^{\pi}[F_a + F_r](Z_c + x\cos y)\cos y dy \\ G = \dfrac{2g}{\omega_1} = 2Q_1\dfrac{\omega-\omega_1}{\omega_1} \end{cases} \quad (27)$$

equation (25) can be written as

$$\begin{cases} \sqrt{1+G^2}\,\sin\theta = Si_0^{[F_a-F_r]}(Z_c,x) \\ \sqrt{1+G^2}\,\cos\theta = Co_0^{[F_a+F_r]}(Z_c,x) + \dfrac{x}{d}G \end{cases} \quad (28)$$

Well known formulas can be derived from (25) or (28): Cleveland et al. [4] formula that relates phase and dissipation in AM AFM is equivalent to the first equation of (25) with $g$=0 and effective parameters used in [4] calculated based on the physical parameters defined in this paper; Sader & Jarvis [5] formula for relative frequency shift and Garcia & Perez [6] formulas for frequency shift in FM mode are equivalent to the second equation of (25) with $\theta$=$\pi$/2. In their formulas we should use $F = (F_a + F_r)/2$ and $k = m\omega_1^2 = \omega_1^2\rho S\left\|Z_1^1\right\|^2$.

## IV. About Tip-Sample Interaction

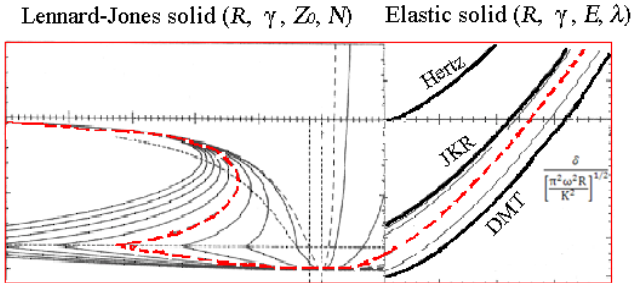


Figure 3. Match of Lenard-Jones and elastic solid models by fitting parameter $N$ and $\lambda$

AFM tip-sample interaction is very critical for interpretation of experimental results, and so it is a topic of intensive experimental and theoretical study. For the purpose of this paper we use Lenard-Jones solid and elastic solid models. Lenard-Jones potential is a model of interaction on the molecular level. Attraction force per unit area between two parallel plates and related potential can be computed by integration [15, p. 31]. Then, using Derjagin approximation, the force between a parallel layer and the spherical tip of molecules can be modeled by the following formula

$$F(z) = 2\pi R\frac{8\gamma}{3}\left[\frac{1}{4}\left(\frac{Z_0}{z}\right)^8 - \left(\frac{Z_0}{z}\right)^2\right] \quad (29)$$

where [15, p. 31] $z$ is the distance between the layer and the tip; and the parameters are: $Z_0$ is the equilibrium distance, $\gamma$ is a half of the work of adhesion, and $R$ is the radius of the tip. Realistic correction to model (29) for molecular multilayers such that $N$/2 layers are free to move has been described in [15, p. 39-45]. The graphs of this model for different $N$ are shown in the left part of Figure 3 and demonstrate the effect of adhesive avalanche [15] which is one of the (many) reasons of dissipation when approach curve $F_a$ may be different from reproach one $F_r$. This is one of the "jump to contact" models. The combination of Lenard-Jones, Derjagin approximation and adhesive avalanche describes the tip-sample interaction before and slightly after the point of geometrical contact.

Mechanical (elastic and elasto-adhesive) contact is described by elastic solid models (Hertz [15, p.245], JKR [15, p. 272, 269] and DMT [15, p. 238]). These models depend on radius of the tip $R$, work of adhesion $2\gamma$ and reduced elastic modulus $E^*$. JKR-DMT transition is parameterized by $\lambda$ [15, p.290-292], see the right part of the graph in Figure 3. Some generalizations of these models for the tips with arbitrary axi-symmetrical profiles are presented in [16]. These elastic-adhesive models describe the tip-sample interaction after and slightly before the point of geometrical contact.

It seems natural to match the Lenard-Jones solid curves with the elastic solid curves in the area slightly before and slightly after the point of geometrical contact where both models are valid. This match is demonstrated in Figure 3 (red dashed line) and can be implemented algorithmically on experimental curves by fitting parameters $N$ and $\lambda$. This match provides a consistent and theoretically justified model of tip sample interaction from tip approaching the surface to a dip penetration of the tip.

## V. Classification of Dynamic AFM Control Modes

System of equations (28) and its extended form (25) are the steady state equations for AFM asymptotic dynamics (24) with dynamic states $x$ –amplitude, and $\theta$ -phase. Two equations of (28) have four unknowns: amplitude $x$, phase $\theta$, base position $Z_c$ usually called height, and variable $G$ proportional to relative frequency shift defined by (27). "Free" oscillation amplitude $d$ is assumed constant, however it can be considered as fifth unknown (in this case usually $x$ assumed constant). To solve two equations of (28), two of the four unknowns should be kept constant and this provides 6 possible combinations. Each combination relates to a potential AFM dynamic control mode and four of these modes are widely used as will be shown below.

In practice two unknown variables are kept constant by feedback control. However, in this paper we assume that feedback control is instant and ideal. This allows avoiding dealing with complications of feedback implementation and concentrating on definition of the dynamic control modes and their properties.

The four widely used dynamic control modes are

1) **Amplitude Modulation (AM): $G$=const (usually G=0 -resonance)**
   a) **AM Spectroscopy mode: $G$ and $Z_c$=const; for each $Z_c$ $x$=$A$ and $\theta$ are calculated respectively for amplitude curve $A$ versus $Z_c$ ($A$v$Z$) and for phase curve $\theta$ versus $Z_c$ ($\theta$v$Z$).**
   b) **AM Imaging mode: $G$ and $x$=$A$=const (amplitude set-point). At each sample position $XY$ the tip-sample interaction defines $F_a$ and $F_r$ in (25); solutions $Z_c$ versus $XY$ give height image and $\theta$ versus $XY$ – phase image - the main data channels for AM.**
2) **Frequency Modulation (FM): $\theta$=const (usually $\theta$=$\pi$/2 –resonance)**
   a) **FM Spectroscopy mode: $\theta$ and $Z_c$ = const; $G$ versus $Z_c$ – frequency shift curve; $x$=$A$ versus $Z_c$ – amplitude curve.**
   b) **FM Imaging mode: $\theta$ and $G$ = const; for each $XY$ point of the sample tip-sample force determines $F_a$ and $F_r$ in (25); solutions $Z_c$ versus $XY$ give height image; and $x$=$A$ versus $XY$ –amplitude image - the main data channels for FM.**

## VI. Interplay with Theory and Experimental Results

In this section simulation of AM AFM based on equation (28) or (25) will be compared with experimental results in different modes classified in Section V.

### A. AM Spectroscopy Mode: AvZ and θvZ curves

The $A$v$Z$ and $\theta$v$Z$ curves, which are simulated for a non-dissipative case, are presented in Figure 4 (top). Some of the data were reported in [17]. Different solutions (branches) for amplitude and phase dependencies on Z are marked with different colors. On a sample approach to the oscillating probe (the distance changes from right – large Z to left - small Z) the system accommodates at the green branch (L) with amplitude and phase both gradually diminishing. As Z is changing a saddle-node bifurcation in amplitude/phase coordinates can happen and the system will jump to the black branch (H). The reverse transition is expected at lower Z. This behavior well matches to the experimental curves obtained on Si substrate, Figure 4 (bottom). The locations with the abrupt transitions are marked with the yellow and red circles. The most drastic changes are observed for the $\theta$v$Z$ curves and they are also related to the transition of the tip-sample forces from the attractive to repulsive range.

When a dissipative case of adhesive avalanche [15] was considered, the main features of the simulated curves remained the same as in the non-dissipative case yet their shape has changed, Figure 5. Experimental data obtained on polymer samples are consistent with these theoretical predictions although variations were observed depending on type of sample, stiffness of the probe and tip size. In some cases such as operation at small amplitudes and imaging of sticky materials the amplitude and phase response behave according to the green branch solution. The abrupt changes of the phase curves and the kinks on the amplitude curves, which are consistent with the transition from the green branch (L) to the white branch (H), were also often detected. Red branch (U) is unstable and so never detected by experiment; it is important, however, to describe the bifurcations.

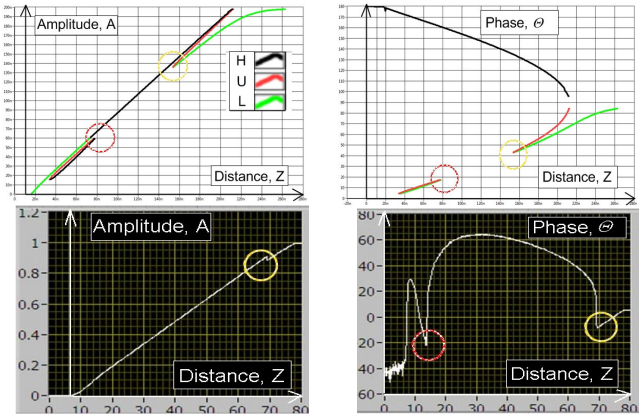


Figure 4. Simulated (upper plots) and experimental (lower plots) $A$v$Z$ and $\theta$v$Z$ curves. Simulations were done for the conservative case. Three branches (H, L - high and low amplitude branches; U - unstable branch) and bifurcations are shown. The measurements were performed on Si substrate.

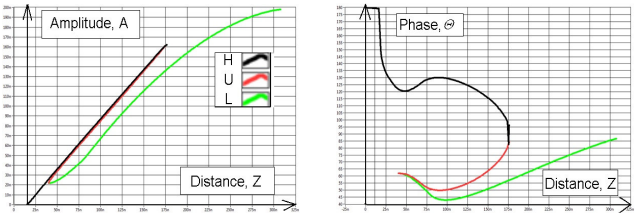


Figure 5. Simulated $A$v$Z$ and $\theta$v$Z$ curves for dissipative case of adhesive avalanche. H, L, U and bifurcation are shown.

### B. AM Imaging Mode

Simulation of the images in different AFM modes might shed light on many outstanding problems of these techniques related to experiments at different forces and use of probes of various geometries and tip dimensions. We have initiated the interplay between the experimental images and simulations using a crystal of polydiethylsiloxane as an example. This sample is often used for demonstration of high-resolution imaging in oscillatory modes. The sketch of the crystallographic structure of the $bc$-plane of this crystal and one of the experimental images of the same crystal surface are shown in Figure 6. The image shows a similar periodical pattern with the periodicities matching the crystal unit cell. In other images one can also see differences of the fine structure inside the unit cell. There are a number of reasons for these

variations, and the simulation of the images is invaluable for their recognition and possible elimination.

The simulated images, which were obtained using Hertz model for tip-sample force interactions, are presented in Figures 7A-D. The pattern in Figure 7A was simulated for imaging with an atomically sharp probe at an extremely low force. Only at such a condition the image mimics the expected crystallographic structure of the sample (Figure 7E). The image in Figure 7B was obtained at the same force but with the 5-nm tip - the practical limit for commercial AFM probes. This results in smearing of the unit cell details. The main repeat distances did not change much and they are within the limits (~5%) of AFM accuracy (not-perfect piezo-scanners).

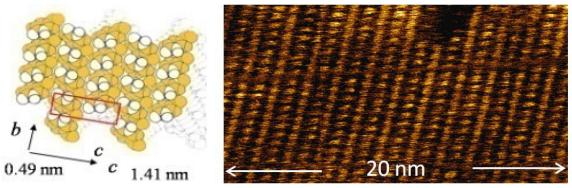


Figure 6. A sketch of the *bc*-plane of polydiacetylene crystal (left) and the image of this plane in the AM mode (right).

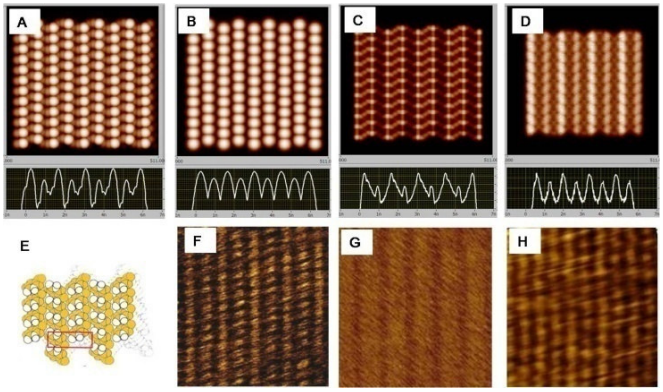


Figure 7. Top row: Simulated AFM images of polydiacetylene crystal at different forces and with tips of different size. Cross-sections along the horizontal direction in the images are shown underneath. Bottom row: the X-ray structure of the surface and experimental AFM images obtained in AM mode match the top row simulated images if blurred by noise.

Surprisingly, the patterns generated for imaging at elevated force and with larger tips (Figures 7C-D) exhibit periodic features inside the crystal unit cell yet their nature has nothing to do with fine structure of the sample. The cross-section profile of the image simulated for 15-nm tip (Figure 7D) exhibits 8 peaks that are less than 9 peaks seen in the profiles of Figures 7A-C. This is another example of bifurcations that complicate AFM studies. These results and the data obtained in simulation of images with single defects [18] confirm that sharp probes and operation at low forces are the required conditions for high-resolution AFM studies and for registration of images with the fake-free contrast and features.

The practically relevant case was explored by the simulation of imaging with double tips. Figure 8 shows a set of images of the crystal obtained for probes with double tips oriented along the horizontal (top patterns) and vertical (bottom patterns) directions. As the tips' size increases from 150 pm (left) to 1 nm (middle) and to 5 nm (right) the pattern becomes more consistent with the unit cell of the crystal. This result is another confirmation that the interpretation of the AFM images of periodical structures in the molecular and atomic scale is an extremely challenging task.

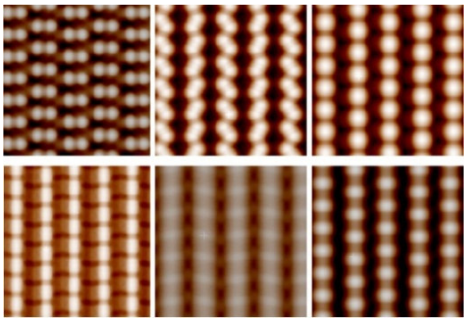

Figure 8. Simulated AFM images of polydiacetylene crystal obtained with probes having double tips.

## VII. SUMMARY

Theoretical analysis of oscillatory AFM modes was performed in a rigorous way using the Euler-Bernoulli equation of the cantilever and asymptotic KBM averaging method for the tip motion. The amplitude modulation (AM) and frequency modulation (FM) modes are classified among other potential modes in the framework of this approach. Simulation of amplitude and phase curves as well as AFM images shows close match with the experimental data. A broad use of this method in the interplay with experimental results will be indispensable for more thorough verification of AFM capabilities and their further progress.

## ACKNOWLEDGEMENT

This work was supported in part by NIST Advanced Technology Program #70NANB4H3055.

## REFERENCES

[1] G. Binnig, C. F. Quate and Ch. Gerber, *Phys. Rev. Lett.* **1986**, *56*, 930.
[2] Y. Martin, C.Williams, H.Wickramasinghe, *J. Appl. Phys.* **1987**, *61*, 4723.
[3] T. Albrecht, P. Gruetter, D. Horne, D. Rugar, *J. Appl. Phys.* **1991,** *61*, 668.
[4] J. Cleveland et al *Appl. Phys. Lett.* **1998**, *72*, 2613
[5] J. E. Sader, S. P. Jarvis *Appl. Phys. Let.* **2004**, *84*, 1801
[6] R. Garcia, P. Perez *Surf Sci Rep* 2002, *47*, 1997
[7] R. W. Stark, W. M. Heckl, *Rev. Sci. Instrum.* **2003**, *74*, 5111.
[8] O. Sahin. S. Magonov, C. Su, C. F. Quate, O. Solgaard, *Nature Nanotechnology* **2007**, *2*, 507.
[9] A. F. Sarioglu, O. Solgaard *Appl. Phys. Lett.* **2008**, *93*, 023114.
[10] R. Stark, N. Naujoks, A. Stemmer, *Nanotechnology* **2007**, *18*, 0655023.
[11] J. Alexander, S. Magonov, M. Moeller, *J. Vac. Sci. Techn. B* **2008**, submitted.
[12] S. Magonov, J. Alexander "Exploring Measurements of Local Electric Properties" Application Note, Agilent Technologies, September **2008**.
[13] S. Timoshenko, *Vibration Problems in Engineering*, 3rd ed., Wolfenden Press, 2007.
[14] N. Krylov, N. Bogolubov, Introduction *to Non-Linear Mechanics*, Princeton University Press, 1949.
[15] D. Maugis, *Contact, Adhesion and Rupture of Elastic Solids*, Springer, 2000.
[16] S. Belikov et al. *J. of Phys.: Conf. Series* **2007**, *61*, 1303.
[17] S. Belikov, N. Erina, S. Magonov, *J. Phys.: Conf. Series* **2007**, *6*, 765.
[18] S. Belikov, S. Magonov *JJAP* **2006**, *45*, 2158.